View metadata, citation and similar papers at core.ac.uk

brought to you by CORE

provided by Brunel University Research Archive

QoS-Constraints and Pilot-Contamination in the Uplink of Non-cooperative Cellular Massive-MIMO

Ismail Hburi[1] and Hamed Al-Raweshidy[2],

Department of Electronic and Computer Engineering

College of Engineering, Design and Physical Sciences, Brunel University London

***Abstract*—This paper investigates the statistical-queueing constraints and pilot contamination phenomenon in random or irregular cellular massive multiple-input-multiple-output (MIMO) system where base stations are Poisson distributed. Specifically, analytical expressions for the asymptotic signal-to-interference-ratio (SIR) coverage, rate-coverage and effective capacity under quality of service (QoS) statistical-exponent constraint are provided for uplink transmission when each base station deploys a large number of antennas. We show that the QoS constrained capacity is in proportional to the path-loss exponent and inversely proportional to the pilot reusing probability which in turn is a function of cell load.**

Our simulation results prove that, pilot reuse impairments can be alleviated by employing a cellular frequency-reuse scheme. For example, with unity frequency reuse factor, we see that, 40% of the total users have SIR above $-10.5dB$, whereas, with frequency reuse factor of $\Omega = 7$, the same fraction of users has SIR above $20.5dB$. However, this can reduce the effective bandwidth of overall system, e.g., for 15% level, the rate drop is almost $10Mbps$ due to using reuse factor of $\Omega = 7$.

***Index Terms*— Cellular massive MIMO, poisson process, log-normal shadowing, coverage probability, effective capacity.**

I. Introduction

The large scale multi-user multiple-input-multiple-output (MU-MIMO) technique is introduced as a promising technique for the fifth-generation (5G) radio systems [1]. Where recent researches validate that base stations (BSs), deploy an order of magnitude more antennas than scheduled-users, have great capability to enhance the throughput and spectral-efficiency (SE) of cellular systems and consequently, meet the fast growth in wireless-traffic of various multimedia-applications. However, the major challenge is the contamination of channel-estimate due to reusing the same pilots in nearby cells and this impairment is termed as pilot-contamination.

A. Related works

Most of the emerging real time applications imposed stringent constraints on queue lengths or queuing delays of transmit buffer. The effective capacity quantifies the maximum arrival rate that can be achieved w.r.t a given service demands with steady-state flow of data at buffer input. In this concern, authors in [2] analysed the effective capacity in single-antenna communication systems. In [3], the effective capacity of Gaussian block-fading MIMO systems is investigated. Moreover, [4] examined in detail, the relationship between the buffer-queuing constraints and MIMO spatial-dimensions. In reference [5], the effective throughput of MIMO systems is investigated over $\kappa-\mu$ fading channels under quality of service (QoS) delay constraints.

On the other hand, many studies have been conducted to address the impact of pilot contamination on statistical distribution of SNR in forward and reverse radio links. The authors in [6], studied the impact of pilot-contamination on the asymptotic distribution of SIR. Thomas L. Marzetta, in [7] considered regular hexagonal-cell topology and uniformly-distributed users. Reference [8] proposed a user-Scheduling algorithm in which the aged channel-state information (CSI) can be used to enhance the spatial multiplexing-gain. Heath et al, in [9], proved that, though bounded by pilot-contamination, large scale MIMO systems can provide significantly higher performance than the systems with single-antenna.

B. Contributions

Motivated by the fact that Pilot-contamination is the main limiting-factor in large antenna regimes [7], we seek in this paper to address the challenge as well as the statistical-queueing constraints in uplink massive-MIMO wireless systems and investigate some key metrics such as SIR-outage, rate-outage and effective-capacity.

Unlike the regular topology considered in prior work [7], we examine irregular topology of cellular massive MIMO which is known to be closer to practical demand-based deployment of BSs. Moreover, different from [9], we consider the QoS constraints and the effective capacity performance which offers a suitable metric to assess the implications that physical layer design may have on link layer performance. Such cross layer analysis could play a key role in 5G systems designing. The specific contributions of this work can be summarized as follows,

1) We characterise the uplink's asymptotic SIR coverage probability, rate coverage and effective capacity of a large antenna-array regime when the BSs are deployed according to poison point process (PPP) distribution. Crucial expressions are obtained (closed-form or analytical formula) in terms of benchmarking the performance of a randomly selected user (typical user) in the cellular network.
2) We evaluate the implications of channel and system parameters on the uplink performance via numerical analysis with remarkable comments. The provided precise approximation results can replace the need for lengthy-

Monte-Carlo simulations in designing of large scale MIMO systems.

II. Assumptions and System Model

We consider the uplink of a non cooperative cellular multi user time division-duplex (TDD) massive-MIMO system. In our mathematical-formulation, we leverage the following assumptions. For the BSs layout, we assume homogeneous Poisson Point Process (PPP) Φ_b of density λ_b on the plane which provides further tractability from stochastic geometry tools. Each BS is equipped with M antennas and randomly allocated ,with equal probability, one of Ω different frequency bands. The number of, one-antenna, users (UEs) associated with a BS follow a homogeneous PPP Φ_u with intensity of λ_u. The UEs' locations are assumed to follow uniform distribution in a disc of radius R_o and uncorrelated with the distribution of other cells users.

A. Estimating Uplink-Channel

For acquiring channel state information (CSI), we consider pilot-based channel-estimation in which all the users send pre-assigned training-sequences (from orthonormal pilot set $\{\Phi_p\}_{p=1}^{P}$) each of length τ to their BSs. The pilot set is assumed to be reused among all cells. Leveraging channel estimates, BSs apply a maximum ratio combining (MRC) to recover received uplink data. The received pilot signals at the serving base station (BS_b) can be written as

$$\mathbf{Y}_b = \sqrt{p_u}\sum_{l=1}^{\infty}\sum_{p=1}^{P}\alpha_{bl}\mathbf{G}_{blp}\mathbf{S}_l^H\chi_{lp} + \mathbf{n}_b \tag{1}$$

where, M is the number of BS antennas, b is the typical or serving BS index, l is the cell index, p is the pilot index, p_u is signal to noise ratio (SNR) of the pilot, $\mathbf{G}_{blp} = h_{blp}\sqrt{\beta_{blp}/r_{blp}^{\nu}}$, $\mathbf{G}_{blp} \in \mathbb{C}^{M\times 1}$ is the channel vector from interfering user (UE_lp) to BS_b, $h_{blp} \in \mathbb{C}^{M\times 1}$ models the small-scale fading vector with i.i.d. zero mean and unit-variance entries, r_{blp} denotes the distance between UE_lb and BS_b, ν is the path-loss-exponent, $\beta_{blp} \sim LogNormal(0, \sigma_{dB}^2)$ is the long-term shadow fading coefficients, $\mathbf{S}_l$ is the pilot symbol transmitted by UE_lp, the superscript-H denotes conjugate-transpose and $\mathbf{n}_b \sim \mathcal{CN}(0,1)$ denotes the AWGN-noise received at BS_b's antennas. The factor α_{bl} accounts for the frequency reuse probability between the typical and interfering BSs,

$$\alpha_{bl} = \begin{cases} 1 & \text{if } \text{BS}_\text{b} \text{ and } \text{BS}_\text{l} \text{ employ the same frequency band.} \\ 0 & \text{Otherwise .} \end{cases}$$

The factor χ_{lp} in eq.(1) accounts for pilot reuse probability by a particular interfering BS_l,

$$\chi_{lp} = \begin{cases} 1 & \text{if } \text{BS}_\text{l} \text{ uses the p-th pilot sequence.} \\ 0 & \text{Otherwise .} \end{cases}$$

According to the received signal (1), BS_b estimates the channel gain of the terminal transmitting the *p-th* pilot sequence,

$$\hat{\mathbf{G}}_{bbp} = \frac{1}{\sqrt{p_u}}\mathbf{Y}_b\mathbf{S}_b \overset{(a)}{=} \mathbf{G}_{bbp}\mathbf{S}_b^H\mathbf{S}_b + \sum_{l=1}^{\infty}\sum_{p=1}^{P}\alpha_{bl}\mathbf{G}_{blp}\mathbf{S}_b^H\mathbf{S}_b\chi_{lp} + \frac{\mathbf{n}_b\mathbf{S}_b}{\sqrt{p_u}}$$
$$\overset{(b)}{=} \mathbf{G}_{bbp} + \sum_{l=1}^{\infty}\sum_{p=1}^{P}\alpha_{bl}\mathbf{G}_{blp}\chi_{lp} + \frac{\mathbf{n}_b\mathbf{S}_b}{\sqrt{p_u}} \tag{2}$$

where, $\mathbf{G}_{bbp}$ is the required or desired channel, (a) follows by substituting for $\mathbf{Y}_b$ from (1), (b) follows due to employing orthogonal pilot sequences. The second term in (b) is the contamination due to pilot reusing by the users associated with other cells[1] and the last term represents the background-noise.

B. Reverse-link Signal

The estimation phase is followed by uplink data transmission phase, where all the UEs transmit useful data-symbols to their BSs. The reverse-link baseband signal at BS_b can be expressed as, $\mathbf{y}_b = \sqrt{p_b}\sum_{l=1}^{\infty}\sum_{p=1}^{P}\alpha_{bl}\mathbf{G}_{blp}\mathbf{u}_l^H\chi_{lp} + \mathbf{n}_b'$, where, p_b is the signal SNR, $\mathbf{u}_l$ represents uplink data symbols of cell-l and $\mathbf{n}_b' \sim \mathcal{CN}(0,1)$ denotes the AWGN-noise. Uplink data can be recovered by left multiplying the received signal by the conjugate transpose of the channel-estimate (2) of the required terminal, i.e., passing through MRC-detector,

$$\hat{\mathbf{u}}_{lb} = \lim_{M\to\infty}\frac{\hat{\mathbf{G}}_{bbp}^H\mathbf{y}_b}{M\sqrt{p_b}} \overset{(a)}{=} \lim_{M\to\infty}\frac{1}{M\sqrt{p_b}}\left[\mathbf{G}_{bbp} + \sum_{l=1}^{\infty}\sum_{p=1}^{P}\alpha_{bl}\mathbf{G}_{blp}\chi_{lp} + \frac{\mathbf{n}_b\mathbf{S}_b}{\sqrt{p_u}}\right]^H$$
$$\cdot\left[\sqrt{p_b}\sum_{m=1}^{\infty}\sum_{n=1}^{P}\alpha_{bl}\mathbf{G}_{bmn}\mathbf{u}_l^H\chi_{mn} + \mathbf{n}_b'\right] \tag{3}$$

where (a) follows due to substituting for $\hat{\mathbf{G}}_{bbp}$ and $\mathbf{y}_b$. Now, we can simplify the expression in (3), leveraging the fact that entries of $\mathbf{n}_b$ and h_{blp} are i.i.d. random variables with zero-mean and unit-variance. Hence, exploiting the strong law of large-numbers (SLLN), only the products of identical-quantities in (3) remain significant [7]. So, for identical-quantities we have

$$\lim_{M\to\infty}\frac{\mathbf{G}_{blp}^H\mathbf{G}_{bmn}}{M\sqrt{p_u}} = \frac{(\beta_{blp}\beta_{bmn})^{1/2}}{(r_{blp}r_{bmn})^{\nu/2}}\lim_{M\to\infty}\frac{h_{blp}^H h_{bmn}}{M\sqrt{p_u}} = \frac{\alpha_{bl}\,\beta_{blp}}{r_{blp}^{\nu}}\,\delta(lm) \tag{4}$$

where $\delta(x)$ is the Dirac-delta function. On the other hand, for non-identical-quantities we have

$$\lim_{M\to\infty}\frac{\mathbf{n}_b^H h_{bmn}}{M\sqrt{p_u}} = \lim_{M\to\infty}\frac{\mathbf{n}_b^H\mathbf{n}_b'}{M\sqrt{p_u}} = \lim_{M\to\infty}\frac{h_{blp}^H\mathbf{n}_b'}{M\sqrt{p_u}} = 0 \tag{5}$$

Using (4) and (5), we can simplify (3) as,
$\hat{\mathbf{u}}_{bp} = \frac{\beta_{bbp}}{r_{bbp}^{\nu}}\mathbf{u}_{bp} + \sum_{l=1}^{\infty}\sum_{p=1 l\neq b}^{P}\frac{\alpha_{bl}\,\beta_{blp}\,\chi_{lp}}{r_{blp}^{\nu}}\mathbf{u}_{lp}$, which reveals the typical and appealing traits of massive-MIMO systems.

III. Asymptotic interference distribution

The typical BS_b in consideration is assumed to be at the origin of the plane as shown in fig.1. UEs are uniformly distributed in each cell and the locations of all the interfering users sharing the same pilot-sequence are assumed to form an independent poison point process on $\mathbb{R}^2$.

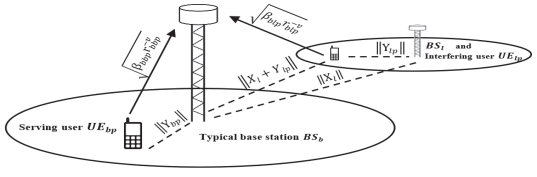

Fig. 1. System parameters of the adopted reverse link model. Where, $Y_{lp} \in \mathbb{R}^2$ is the cartesian coordinates location of the interferening user UE_{lp} w.r.t its basestation BS_{lp}, $X_l \in \mathbb{R}^2$ is the cartesian coordinates location of basestation BS_{lp} w.r.t BS_{bp}, r_{lbp} is the polar coordinates representation of the distance $\|X_l + Y_{lp}\|$.

[1] Note that, since same set of pilot-sequences are reused among all the BSs, so index subscript can be dropped from the symbol $\mathbf{S}_b$.

LEMMA.1 (Interference Characteristic) *Invoking the basic formula of L.T, the uplink interference at the typical BS can be characterised as follows*

$$\begin{aligned}\mathscr{L}_{I_{bp}}(s) &= \mathbb{E}_{I_{bp}}\{e^{-sI_{bp}}\} \overset{(a)}{=} \mathbb{E}_{\beta_{blp},r_{blp}}\left\{\exp\left[-s\textstyle\sum_{l\in\mathcal{B}\setminus\{b\}}\dfrac{\alpha_{bl}\,\beta_{blp}^2\,\chi_{lp}}{r_{blp}^{2\nu}}\right]\right\}\\ &\overset{(b)}{=} \mathbb{E}_{\beta_{blp},r_{blp}}\left\{\textstyle\prod_{l\in\mathcal{B}\setminus\{b\}}\exp\left[-s\dfrac{\alpha_{bl}\,\beta_{blp}^2\,\chi_{lp}}{r_{blp}^{2\nu}}\right]\right\}\\ &\overset{(c)}{=} \exp\left[\frac{-2\pi\lambda_b\,\bar{\chi}}{\Omega}\mathbb{E}_{\beta_{blp}}\left\{\int_{r\in\mathbb{R}^+} r\left(1-e^{-s\,\beta_{blp}^2 r^{-2\nu}}\right)dr\right\}\right]\\ &\overset{(d)}{=} \exp\left[\frac{-\pi\lambda_b\,\mathbb{E}\{\chi_{lp}\}\;s^{\frac{1}{\nu}}}{\Omega}\mathbb{E}\left\{\beta_{blp}^{\frac{2}{\nu}}\right\}\underbrace{\int_{x\in\mathbb{R}^+}\left(e^{-x^{-\nu}}-1\right)dx}_{I_1}\right] \quad (6)\end{aligned}$$

where, (a) is obtained by substituting for I_{bp} which is the inter-cell interference ICI, i.e., the sum of powers from all interfering users of other cells except cell-b (orthogonal pilot sequences assumption implies no intra-cell interference), $\alpha_{bl} \in \{0,1\}$ is a Bernoulli random variable with mean $1/\Omega$, i.e., $\alpha_{bl} \sim$ *Bernoulli*$(\frac{1}{\Omega})$. Which implies that α_{bl} takes value of one if the serving $\mathrm{BS_b}$ and interfering $\mathrm{BS_l}$ share the specified frequency sub-band and $\mathcal{B}$ is the set of all the cells in the cellular system. (b) follows since exponential of a sum is a product of exponential. (c) follows from probability generating function of the Poisson point process (PGFL), given that $\mathbb{E}\{\prod_{x\in\Phi} v(x)\} = \exp\big[-\lambda_b\int_{\mathbb{R}^2}\big(1-v(x)\big)dx\big]$, converting into polar coordinates gives, $\mathbb{E}\{\prod_{x\in\Phi} v(x)\} = \exp\big[-2\pi\lambda_b\int_{\mathbb{R}^+}\big(1-v(r)\big)dr\big]$, and then averaging out the Bernolli r.v. α_{bl}, where each cell is randomly-allocated one of the Ω sub-bands (frequency reuse factor), so the interference is thinned with a reuse-factor of Ω. Finally, (d) is obtained by setting $x = s^{-1/\nu}\beta_b^{-2/\nu}\,r^2$, evaluating the expectation over β_{blp}, assuming $\{\beta_i\}_{i=0}^{\infty}$ is a set of i.i.d. unit mean exponential random variables satisfy $\mathbb{E}[\beta_{blp}^{2/\nu}] < \infty$.

LEMMA.2 (Pilot Reuse Probability) *The expectation over the probability of pilot reusing χ_{lp} can be obtain as follows*

$$\mathbb{E}\{\chi_{lp}\} = \frac{\mathbb{E}_{k\geq P}[k]}{P}\;\mathbb{P}\{k<P\} + \mathbb{P}\{k\geq P\} \quad (7)$$

where, k is the number of active users associated with base station BS_l. The first term accounts for the case when $\{k < P\}$ hence, there exists a probability that the interfering base station BS_l doesn't use the *k*th pilot-sequence. The second term stands for the case when $\{k \geq P\}$, i.e., all the available pilot-sequences will be used by the interfering base station. It's worthwhile to note that k is a r.v. associated with the size-distribution of Voronoi-cell corresponding to BS_l which has no-known accurate distributions. However, the distribution can be approximated using gamma distribution,accordingly, (7) can be re-written as

$$\mathbb{E}\{\chi_{lp}\} = \textstyle\sum_{k=1}^{P-1}\dfrac{1}{P}\dfrac{(\lambda_u\pi R_o^2)^k}{(k-1)!}\,e^{-\lambda_u\pi R_o^2} + \sum_{k=P}^{\infty}\dfrac{(\lambda_u\pi R_o^2)^k}{(k)!}\,e^{-\lambda_u\pi R_o^2}$$

Next, we evaluate the integration I_1 in (6-d) with the help of the following identities, $\{\Gamma(1+z) = z\,\Gamma(z)\}$, $\{\Gamma(1-z) = 1/\Gamma(1+z)\,\mathrm{sinc}(\pi z)\}$ and $\{\int_0^{\infty} x^{\nu-1}(1-e^{-\mu x^p})\mathrm{dx} = -\dfrac{1}{|p|}\,\mu^{-\nu/p}\,\Gamma(\frac{\nu}{p})\}$, which result in $I_1 = \int_{\mathbb{R}^+}\big(e^{-x^{-\nu}}-1\big)dx = \dfrac{1}{\Gamma(1+\frac{1}{\nu})\,\mathrm{sinc}(\frac{\pi}{\nu})}$, plugging again into (6-d) yields

$$\mathscr{L}_{I_{bp}}(s) = \exp\left[-\frac{\pi\,\lambda_b\,\mathbb{E}[\beta_{blp}^{2/\nu}]\,\bar{\chi}\,s^{1/\nu}}{\Omega\,\Gamma(1+\frac{1}{\nu})\,\mathrm{sinc}(\frac{\pi}{\nu})}\right] \quad (8)$$

where, $\bar{\chi} = \mathbb{E}\{\chi_{lp}\}$ is the 1st moment or mean of the r.v χ which can be set to one if we consider a scenario of interfering UEs with full buffer such that all the interferers are always-active. The common assumption for the distribution of shadowing is the log-normal one, in which $\beta_{blp} = 10^{X_{blp}/10}$, given that $X_{blp} \sim \mathcal{N}(\mu_{blp}, \sigma_{blp}^2)$ and $\mu_{blp}, \sigma_{blp}^2$ are, respectively, the "mean" and "standard deviation" of the large-scale channel gain. In this case, the $2/\nu^{th}$ moment can be found, employing the moment-generating function (MGF) of Gaussian-distribution, which is $\mathbb{E}[\beta_{blp}^{2/\nu}] = \exp[\frac{\ln(10)}{5}\frac{\mu_{blp}}{\nu} + \frac{1}{2}(\frac{\ln(10)}{5}\frac{\sigma_{blp}}{\nu})^2]$ and it is finite for $\{\mu_{blp}, \sigma_{blp}\} < \infty$. For exponential-distribution approximation, $\beta_{blp}^2 \sim \exp(\mu_{blp})$ we have $\mathbb{E}[\beta_{blp}^{2/\nu}] = \mu_{blp}^{-2/\nu}\,\Gamma(\frac{2}{\nu}+1)$ and $\Gamma(\frac{2}{\nu}+1)$ is the $2/\nu^{th}$ moment of unit-mean exponential-random variables. Plugging in (8) we obtain L.T of the interference for exponential-approximation shadowing as an immediate consequence of applying independent-thinning on Φ_b given as, $\mathscr{L}_{I_{bp}}(s) = \exp\left[-\frac{\pi\,\lambda_b\,\bar{\chi}\,s^{1/\nu}}{\Omega\,\mathrm{sinc}(\frac{\pi}{\nu})}\right]$, where this function can be used for further system analysis.

IV. PERFORMANCE METRICS

In this section we are going to derive the mathematical expression for some key metrics that characterised system performance.

A. PROBABILITY OF COVERAGE

The probability of coverage can be formally defined as the probability that the uplink $\mathrm{SIR_b^{UL}}$ at the tagged base station $\mathrm{BS_b}$ is greater than the threshold (or target) $\mathrm{SIR_{th}^{UL}}$, $\mathbb{P}\{SIR_b^{UL} > SIR_{th}^{UL}\}$.

THEOREM.1 *For massive-antenna BS's with a homogeneous-ppp distribution of density λ_b and unit mean exponential shadowing, the tail probability of uplink-SIR of a typical user UE for SIR-threshold of T_1 can be mathematically expressed as*

$$\mathbf{P}_{cov}(T_1,\lambda_b,\nu) = \frac{1}{C_1(T_1,\lambda_b,\nu)\,R_o^2}\left[1-\exp(-C_1(T_1,\lambda_b,\nu)\,R_o^2)\right], \quad (9)$$

$$\text{where,} \qquad C_1(T_1,\lambda,\nu) = \frac{\pi\,\lambda_b\,\bar{\chi}\,T_1^{1/\nu}}{\Omega\,\mathrm{sinc}(\frac{\pi}{\nu})} \quad (10)$$

T_1 is the target or level that the SIR must exceed in order to establish a connection. *Proof*: see appendix A □

B. RATE COVERAGE PROBABILITY

Rate-coverage ($\mathrm{R_{cov}}$) for a typical user UE can be defined as the probability that the data rate of this user is larger than a predefined threshold value (lowest-rate) required for a given application.

THEOREM 2 *For massive-antenna BS's with a homogeneous-ppp distribution of density λ_b and unit mean exponential*

shadowing, the tail probability of uplink-rate of a typical user UE for rate-threshold of T_2 can be given by

$$R^{UL}_{cov}(T_2,\lambda_b,\nu)=\frac{1}{C_2(T_2,\lambda_b,\nu)\,R_o^2}\left[1-\exp\left(-C_2(T_2,\lambda_b,\nu)\,R_o^2\right)\right], \quad (11)$$

$$\text{where,} \qquad C_2(T_2,\lambda_b,\nu)=\frac{\pi\,\lambda_b\,\bar{\chi}\,(e^{\frac{\ln(2)\,\Omega\,T_2}{\vartheta B}}-1)^{1/\nu}}{\Omega\,\mathrm{sinc}(\frac{\pi}{\nu})} \quad (12)$$

and ϑ is the pilot and cyclic prefix (CP) overheads factor [7].
Proof: see appendix B □

C. Effective-Capacity

It is noteworthy that the well known Shannon's capacity formula for wireless transmission, cannot account for the quality of service demands. So, a significant figure of merit, namely, effective capacity is introduced to incorporate statistical delay QoS into capacity formula of wireless applications [10]. In this regard, a new parameter θ, relates to the asymptotic decay-rate of the buffer-occupancy can be given by $\theta=-\lim_{x\to\infty}\frac{\ln(Pr\{L>x\}}{x}$, where, L is the queue length at steady-state of the transmitter buffer, x is the delay bound, and Φ is determined by the arrival state and service-processes [11]. According to this equation, θ_k quantities the equilibrium state delay violation-probability of the k-th user. It should be noted that a smaller θ indicates a looser QoS-constraint whereas a larger θ imposes a more stringent constraints. Accordingly, the effective capacity as a function of QoS exponent can be defined as

$$C_{eff}(\theta)=-\lim_{n\to\infty}\frac{1}{n\,T\theta B}\log_2\mathbb{E}_R\left\{e^{-T\theta B\sum_{i=1}^{n}R[i]}\right\} \quad (13)$$

where T is frame-duration and $R_k[i]$ is the transmission rate in the $i-th$ time slot. With no loss of generality, we assume that the fading-process over wireless-channels is independent of each other and holds invariant within a block length T and the service-process is uncorrelated stochastic-process (independent and identically distributed). Hence, C_{eff} in (13) can be simplified to [10], [2] $C_{eff}(\theta)=-\frac{1}{T\theta B}\log_2\mathbb{E}_R\{e^{-T\theta BR}\}$, where, B is system bandwidth and the expectation is taken w.r.t the random variable R_k. Obviously, the effective capacity coincides with the traditional Shannon's ergodic-capacity in case there is no delay-constraint i.e. $\theta\to 0$. Analytically, with the assumption of steady state of the buffer input (stationary and ergodic process), and after substituting for rate R from Shannon's formula, the effective capacity normalized by the bandwidth, will be as follows,

$$C^{UL}_{eff}(t,\lambda_b,\nu,\theta)=-\frac{1}{A}\log_2\mathbb{E}((1+SIR)^{-A}) \quad (14)$$

where, $A\triangleq\theta TB/\Omega\ln(2)$ and the expectation is taken over the distribution of SIR.

THEOREM 3 *For massive-antenna BS's with a homogeneous-ppp distribution of density λ_b and unit mean exponential shadowing, the asymptotic uplink effective-capacity of a typical user UE for threshold of t and QoS exponent θ, can be given by*

$$C^{UL}_{eff}(t,\lambda_b,\nu,\theta)=-\frac{1}{A}\log_2\left[1-\textstyle\sum_{i=1}^{N}\omega_i\,V(x_i)\right]+\mathcal{O}_N \quad (15)$$

where, $V(x_i)$ is the coverage probability (9) replacing T_1 by $\left(t^{-1/A}-1\right)$, the factor N is an integer, represents the number of terms used in the approximation and determines the accuracy of integration. ω_i, x_i are respectively, the weights and abscissas which are determined by Hermite polynomial according to the selected value of N. The symbol $\mathcal{O}_N$ is a remainder term.

Proof: see appendix C □

V. Numerical-Results and Discussion

This section presents the details of numerical validation for the derived analytical results of section (IV) and gives insights into how the various parameters impact the distribution of the performance metrics in the cellular system. Table-I summarizes the specific parameters used in the simulations unless otherwise specified.

a) SIR Profile: First, fig.2-(a) compares the log-normal Monte-Carlo simulated uplink-coverage with the corresponding exponential-analytical formula given in (9) under various frequency reuse factor Ω. We can see that the analytical results almost matches the simulation ones, particularly at large threshold-SIR. Average interferer-distance in the wireless cellular system increases as Ω increases, this helps establish an intuition of why a higher frequency reuse factor has a better SIR tail-probability than lower ones. For instance, we see that, 40% of the users have SIR above $-10.5dB$ with unity frequency reuse factor, whereas the same fraction of users has SIR above $20.5dB$ with frequency reuse factor of $\Omega=7$. The SIR-gain drops when we consider lower or higher-SIR users, but is again significant. Noteworthy that low percentile levels are for cell-edge users while high percentile levels are for cell-center users.

b) Impact of Cell Load: Fig.2-(b) analyses different scenarios based on cells load. It is noticeable that the complementary cumulative distributions of the uplink-SIR degrade in case of fully-loaded cells when each BS serving its maximum-capacity of users, $\bar{\chi}=1\,\text{for}\,K=P$ (high contamination scenario). This is consistent with simple intuition, since increasing the number of served users K means increasing in the pilot reuse probability between the typical and interfering BSs according

Table I. Numerical parameters used in the simulation.

PARAMETERS	SETTING
BS coverage-radius R_o	1,500 m
Cellular area radius R	40 Km
Density of BSs λ_b	$1/\pi\,R_o^2$
Frequency reuse factors Ω	1, 3 and 7
Path-loss-exponent ν	4.0
Large-scale shadowing β_{blp}	$\sim$ Log-normal(μ,σ^2) for simulation
	$\sim$ exp(1) for analytical analysis
Log-normal shadowing μ,σ^2_{dB}	0 , 7 dB respectively
Channel bandwidth	20 MHz
Monte-Carlo trials	10^5 system realizations.
OFDM symbol duration T_s	$500/7\approx 71.4us$, LTE standard [7]
Pilot training overhead T_{ov}	$(T_{slot}-\tau\,T_s)/T_{slot}=3/7$, [7].
Useful symbol duration T_u	$1/15\approx 66.7us$, LTE standard [7]

to the formula in (7). Consequently, this will decrease the average interferer-distance, i.e., increases aggregated interference power. In contrast, best coverage performance is for $\bar{\chi} = 0.25$ (low contamination scenario). On the other hand, the marginal-gain in coverage performance increases with decreasing in cell load.

c) Pilot-reusing Probability: Fig.3 considers the impact of pilot number P used in channel training phase on the probability of reusing the same sequence between the serving and interfering BSs for different cell coverage-radius R_o. The figure shows that for fixed user-density λ_u, the probability of pilot reusing is relatively large for less number of pilot-sequences or larger cell-coverage radius, e.g., when $P = 8\,pilots$, coverage-radius extension from $0.5km$ to $1.0km$ leads to nearly 50% increment in pilot-reuse probability $\bar{\chi}$.

d) Impact of Ω on Rate Profile: The effect of Ω on the uplink rate coverage is investigated in fig.4-(a). Unlike the SIR-tail probability, here the story is different, where the average achievable rate doesn't definitely increase with Ω increasing. In the high reliability-regime when the rate outage-probability goes to zero, the rate coverage gains increase with Ω increasing. In contrast, in the high spectral-efficiency regime, when the rate threshold goes to infinity, increasing Ω will decrease the rate coverage gains. Although, larger Ω means less average interference power, but also it means smaller cell effective-bandwidth, hence, for $R_{th} > 7Mbps$ increasing Ω has negative effect on the rate performance, e.g., we see that, for 15% level the rate drop is roughly $10Mbps$ due to using reuse factor of 7.

e) Impact of $\bar{\chi}$ on Rate Profile: Fig.4-(b), depicts the effect of the pilot reuse probability on the rate-tail probability, which is nearly the same effect as for the SIR-coverage performance. As an example, for the 20^{th} percentile users, the rate performance drops by almost 75% for pilot reuse probability of $\bar{\chi} = 1.0$ as compared to the $\bar{\chi} = 0.25$ scenario. Similar to the SIR-coverage performance, the marginal-gain in average rate increases with decreasing in cell load. The impact of path-loss-exponent (PLE), ν is investigated in more detail in fig.5 for SIR and rate coverages. As ν decreases, the UEs farther-away from the typical BS have a greater contribution to the aggregated interference-power at the this BS, and this leads to a less uplink-SIR and consequently a smaller SIR and rate-tail probability.

f) Effective Capacity: Fig.6-(a) simulates the normalised effective capacity w.r.t different pilot reuse probability, as expected, C_{eff} decreases with $\bar{\chi}$ increasing. Fig.6-(b), according to the analysis of *Theorem 3*, compares the effective capacities for various path-loss-exponent ν, where a better C_{eff} performance is for larger values of ν for the same reasons mentioned before. Moreover, fig.7 demonstrates the functional-relationship among uplink normalized effective capacity C_{eff}^{UL}, path-loss exponent ν and the QoS exponent θ.

g) Shannon Capacity: Finally, the comparison of the effective capacity with Shannon-capacity, $\theta \longrightarrow 0$ is illustrated in fig.8 for various PLE values. As expected, for all cases, the effective-capacity decreases monotonically with the increase of the QoS statistical-exponent θ (more stringent delay QoS-requirements), while the curves tend to flatten and saturate to the Shannon-capacity C_{SH} when θ becomes small enough.

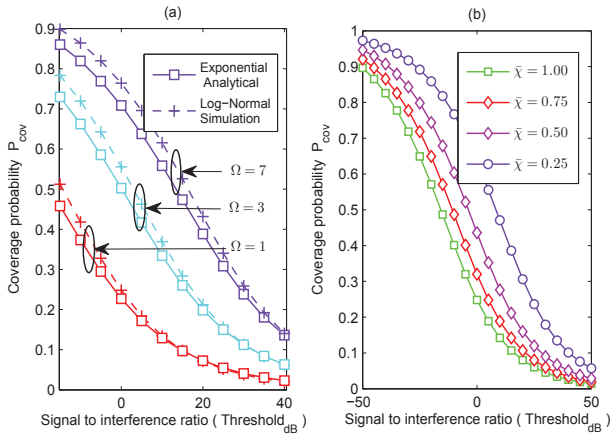

Fig. 2. Uplink Coverage performance of a typical UE, (a) Different frequency band reuse factor. (b) Different pilot reuse probability.

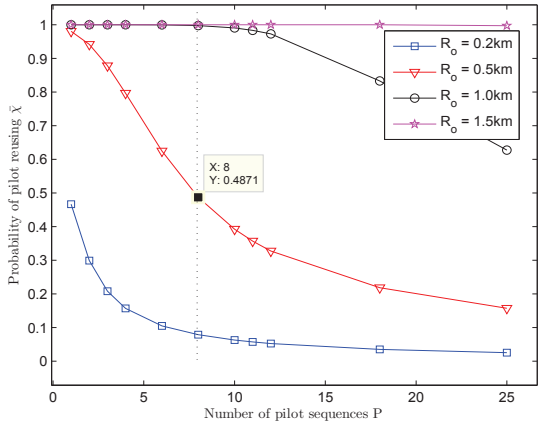

Fig. 3. Pilot reuse probability versus the number of available pilot-sequences P for user density λ_u of $5/km^2$ and various cell coverage-radius R_o.

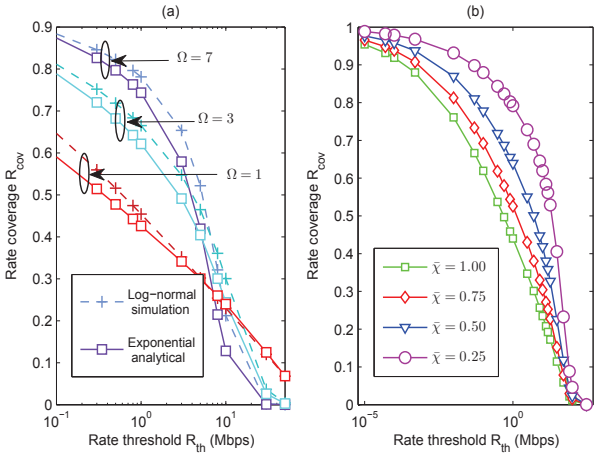

Fig. 4. Uplink Rate-coverage performance of a typical UE, (a) Different frequency band reuse factor. (b) Different pilot reuse probability.

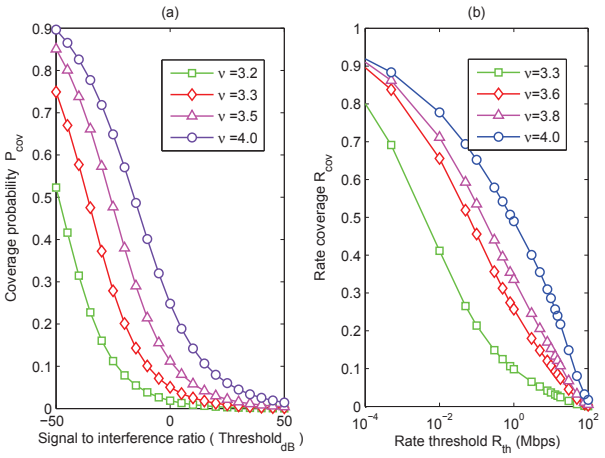

Fig. 5. Path-loss exponent impact, (a) Uplink Coverage probability. (b) Uplink Rate-coverage probability.

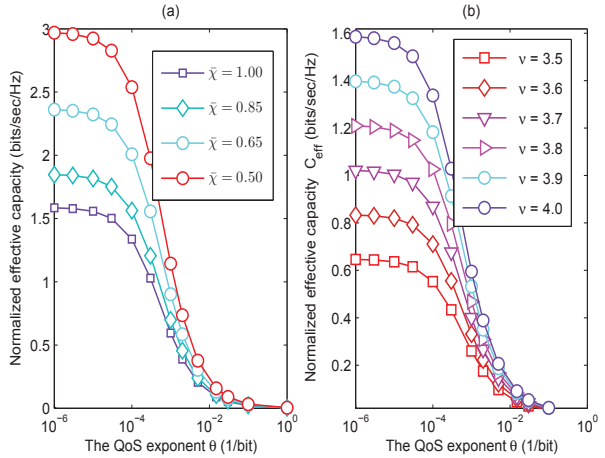

Fig. 6. Uplink normalized effective capacity of a typical UE, (a) Different pilot reuse probability. (b) Different path-loss exponent, (System bandwidth is BW = 0.3MHz, block length is T = 2ms).

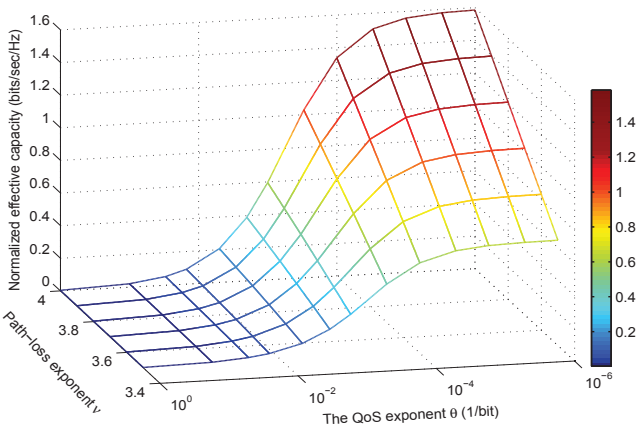

Fig. 7. The functional-relationship among uplink normalized effective capacity C_{eff}^{UL}, path-loss exponent ν and the QoS exponent θ of a typical UE (System bandwidth is BW = 0.3MHz, block length is T = 2ms).

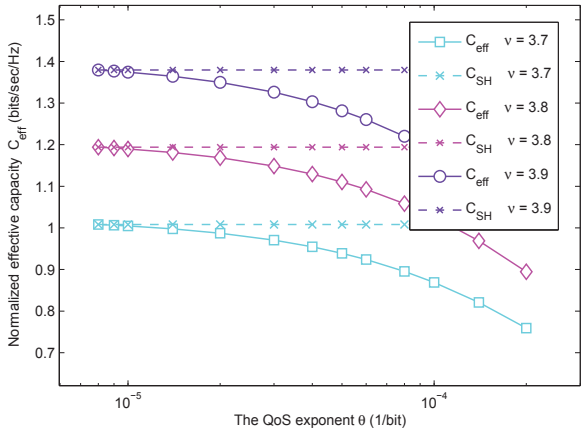

Fig. 8. The behaviour of the normalized effective capacity C_{eff} compared with the Shannon capacity C_{SH}, (System bandwidth is BW = 0.3MHz, block length is T = 2ms).

VI. Conclusion

In this work we provided tractable-expressions for the asymptotic SIR coverage, rate coverage and effective capacity in the uplink of the interference limited cellular massive MIMO. The expressions are based-on a Poisson point process topology using stochastic geometry tools. The presented results provide valuable insight into the impacts of key system-features such as path-loss attenuation, shadowing and pilot-contamination on the statistical distributions of various system metrics. Simulations clearly illustrate that the SIR-coverage performance improves as frequency reuse factor Ω increases due to the increases of distances between the typical and interfering UEs.

However, a trade off is required in Ω selection when a guaranteed minimum-rate is required since increasing Ω will decrease the effective bandwidth. Furthermore, we investigated the impacts of path-loss exponent and the pilot reusing probability, which is a function of the cell-load, on the effective capacity at a typical BS. In this aspect, results show that path-loss in cellular system plays a key role in mitigating the system overall interference and the effective capacity is in proportion to the path-loss attenuation. More practical-issues, like uplink power-control and dynamic frequency reuse scheme, are expected to be addressed in the future analysis.

Appendix-A

Proof of theorem 1: Starting with the formal definition of coverage probability, as the tail Probability of SIR, i.e., ccdf of SIR averaged over the distribution of the users, we have

$$\mathbf{P}_{cov}(T_1,\lambda_b,\nu)=\mathbb{E}_r\Big[\mathbb{P}\{SIR>T_1\}\Big]\overset{(a)}{=}\int_0^{R_o}\mathbb{P}\{SIR>T_1\}f_{R_o}(r)dr \tag{16}$$

Now, we are going to characterize the statistical distribution of SIR in (16) conditioned on user location r_{bbp}

$$\mathbb{P}\{SIR>T_1\}\overset{(a)}{=}\mathbb{P}\Big\{\beta_{bbp}^2>T_1\,r_{bbp}^{2\nu}\textstyle\sum_{l\in\mathcal{B}\setminus\{b\}}\dfrac{\alpha_{bl}\,\beta_{blp}^2\,\chi_{lp}}{r_{blp}^{2\nu}}\Big\}$$

$$\overset{(b)}{=}\mathbb{E}_{I_{bp},\beta^2}\Big\{\exp\Big[-T_1\,r_{bbp}^{2\nu}\textstyle\sum_{l\in\mathcal{B}\setminus\{b\}}\dfrac{\alpha_{bl}\,\beta_{blp}^2\,\chi_{lp}}{r_{blp}^{2\nu}}\Big]\Big\}$$

$$\stackrel{(c)}{=} \mathbb{E}_{I_{bp},\beta^2,r}\Big\{e^{-T_1\, r_{bbp}^{2\nu}\, I_{bp}}\Big\} \stackrel{(d)}{=} \mathbb{E}_{I_{bp},\beta^2}\Big\{e^{-s\, I_{bp}}\Big\} \stackrel{(e)}{=} \mathscr{L}_{I_{bp}}(s), \qquad (17)$$

where, (a) is obtained by substituting for inter-cell interference I_{bp} which is the sum of the powers from all the interfering UEs placed farther than R_o (no intra-cell interference with orthogonal pilot sequences assumption) and re-arrange the inequality variables, (b) follows assuming $\{\beta_i\}_{i=0}^{\infty}$ is a set of i.i.d. unit-mean exponential random-variables, i.e. $\beta^2 \sim \exp(1)$, (c) follows assuming $s = T_1\, r_{bbp}^{2\nu}$ as a constant in Laplace equation and (d) is, by definition, the Laplacian of interference w.r.t to the constant s. Next, substitute for $\mathscr{L}_{I_{bp}}(s)$ from (8) yields, $\mathbb{P}\{SIR > T_1\} = \exp\left[\dfrac{-\pi\, \lambda_b\, \bar{\chi}\, s^{1/\nu}}{\Omega\, \mathrm{sinc}(\frac{\pi}{\nu})}\right]$. Re-setting $s = T_1\, r_{bbp}^{2\nu}$, averaging out the random variable $\mathrm{r_{bbp}}$ and then plugging again into (16) we obtain

$$\mathbf{P}_{cov}(T_1,\lambda_b,\nu) = \mathbb{E}_{r_{bbp}}\left\{\exp\left[\frac{-\pi\, \lambda_b\, \bar{\chi}\, (T_1\, r_{bbp}^{2\nu})^{1/\nu}}{\Omega\, \mathrm{sinc}(\frac{\pi}{\nu})}\right]\right\}$$
$$\stackrel{(a)}{=} \int_0^{R_o}\left\{e^{-C_1(T_1,\lambda_b,\nu)\, r_{bbp}^2}\right\} f_R(r)dr \stackrel{(b)}{=} \int_0^{R_o}\left\{\frac{2r_{bbp}}{R_o^2} e^{-C_1(T_1,\lambda_b,\nu)\, r_{bbp}^2}\right\} dr \qquad (18)$$

In (a), the expectation w.r.t the random variable r_{bbp} expressed in integral form, where $C_1(T_1,\lambda_b,\nu) = \dfrac{\pi\, \lambda_b\, \bar{\chi}\, T_1^{1/\nu}}{\Omega\, \mathrm{sinc}(\frac{\pi}{\nu})}$, (b) follows from substituting for $f_R(r)$, in our scenario, we have uniform user-distribution within disc of radius $\mathrm{R_o}$ such that $f_R(r) = (2r/R_o^2)$ for $r \in (0, R_o]$. Finally, setting $x = r^2$ and evaluating the integration we arrive at (9) which completes the proof.

APPENDIX-B

Proof of theorem 2: Starting from the definition of the normalized average-rate we have [7]

$$R_{cov}^{UL}(T_2,\lambda_b,\nu) = \mathbb{E}\Big\{\ \frac{B\, T_{ov}\, T_u}{\Omega\, T_s}\ \log_2(1+SIR)\Big\} \qquad (19)$$

Given that B is the bandwidth, T_s is the orthogonal-frequency division-multiplexing (OFDM) symbol duration T_s = slot duration/# of symbole per slot, T_{ov} is the pilot overhead or training efficiency, $T_{ov} = \dfrac{(T_{slot} - T_{pilot})}{T_{slot}} = \dfrac{(T_{slot} - \tau\, T_s)}{T_{slot}}$, T_u is the useful symbol duration $T_u = 1/\text{subcarrier spacing} = 1/\Delta_f$, and Ω is the frequency reuse factor (FRF). It's worth pointing out that the pre-log percentage factor ($\dfrac{B\, T_{ov}\, T_u}{\Omega\, T_s}$) implies that the useful data transmission only occupies a fraction of the coherence-slot. The expectation in (19) can be expressed in terms of integration as following (averaging over the SIR distribution)

$$R_{cov}^{UL}(T_2,\lambda_b,\nu) = \int_{r=0}^{R_o}\int_0^{T_2}\mathbb{P}\Big\{\big[\frac{\vartheta\, B}{\Omega}\ \log_2(1+SIR)\ >\ t|r\big] dt\, f_R(r)\Big\} dr$$
$$\stackrel{(a)}{=} \int_{r=0}^{R_o}\int_0^{T_2}\mathbb{P}\Big\{\underbrace{\big[SIR\ >\ (e^{\frac{\ln(2)\,\Omega\, t}{\vartheta\, B}}\ -1)|r\big]}_{\text{SIR-ccdf}}\, dt\, f_R(r)\Big\} dr$$
$$\stackrel{(b)}{=} \frac{1}{C_2(T_2,\lambda_b,\nu)\, R_o^2}\left[1-\exp(-C_2(T_2,\lambda_b,\nu)\, R_o^2)\right], \qquad (20)$$

where, $\vartheta = T_{ov}\cdot T_u/T_s$ accounts for both pilot and cyclic prefix (CP) overheads, the first equality follows exploiting the fact that for a positive r.v. X, data rate in this case, we have $\mathbb{E}[X] = \int_{t>0}\mathbb{P}(X>t)\, dt$, (a) is obtained after re-arrange the inequality variables and (b) follows by substituting for ccdf of SIR from appendix-A, setting $T_1 = \exp(\dfrac{\ln(2)\,\Omega\, T_2}{\vartheta B}) - 1$, substitute for $f_R(r)$ and changing of variables with $x = r^2$, note that $C_2(T_2,\lambda_b,\nu)$ is given by (10), which concludes the proof.

APPENDIX-C

Proof of theorem 3: The normalised effective capacity in (14) can be expressed in terms of the SIR distribution as following $C_{eff}^{UL}(t,\lambda_b,\nu,\theta) = -\dfrac{1}{A}\log_2\int_0^{R_o}\int_0^1\mathbb{P}\Big\{\underbrace{\big[(1+SIR)^{-A}\ >\ t|r\big]dt}_{\mathcal{I}_2}\, f_R(r)\Big\}dr$

Next, $\mathcal{I}_2$ after a simple manipulation will be $\mathcal{I}_2 = \int_0^1\mathbb{P}\big\{\big[SIR\ <\ (t^{-1/A}-1)\big]dt\big\} \stackrel{(a)}{=} 1 - \int_0^1 \underbrace{\mathbb{P}\big\{\big[SIR\ \geq\ (t^{-1/A}-1)|r\big]}_{\text{SIR-ccdf}}\, dt\big\}$, where (a) follows since cdf = 1 − ccdf.

Now, substitute for ccdf from (13) with $T_1 = (t^{-1/A}-1)$ we end-up with the following expression, $C_{eff}^{UL}(t,\lambda_b,\nu,\theta) = -\dfrac{1}{A}\log_2\big[1-\int_0^1(\dfrac{\big[1-e^{-C_3(t,\lambda_b,\nu,\theta)\, R_o^2}\big])}{C_3(t,\lambda_b,\nu,\theta)\, R_o^2}\, dt\big]$,

where $C_3(t,\lambda_b,\nu,\theta) = \dfrac{-\pi\, \lambda_b\, \bar{\chi}\, (t^{-1/A}-1)^{1/\nu}}{\Omega\, \mathrm{sinc}(\frac{\pi}{\nu})}$.

Finally, employing the Hermite approximation for the last integral, we can conclude the proof.

REFERENCES

[1] A. Pitarokoilis, S. K. Mohammed and E. G. Larsson, "On the optimality of single-carrier transmission in large-scale antenna systems," *IEEE Wireless Commun. Lett.,* vol. 1, no. 4, pp. 276–279, Aug. 2012.

[2] J. Tang and X. Zhang, "Quality-of-service driven power and rate adaptation over wireless links," *IEEE Trans. Wireless Commun.*, vol.6, no. 8, pp. 3058–3068, Aug. 2007.

[3] L. Liu and J.-F. Chamberland, "On the effective capacity of multiantenna Gaussian channels," in *Proc. 2008 IEEE Int. Sym. Inf. Theory*,pp. 2583–2587.

[4] M. C. Gursoy, "MIMO wireless communications under statistical queueing constrains,"*IEEE Trans. Inf. Theory*, vol. 57, no. 9, pp. 5897–5917, Sep. 2011.

[5] J. Zhang, Z. Tan, H. Wang, Q. Huang, and L. Hanzo, "The Effective Throughput of MISO Systems over $\kappa-\mu$ Fading Channels," *IEEE Transactions on Vehicular Technology*, vol. 63, no. 2, pp. 943-947, Feb. 2014.

[6] B. Gopalakrishnan and N. Jindal, "An analysis of pilot contamination on multi-user MIMO cellular systems with many antennas," *in Proc. of IEEE 12th International Workshop on Signal Processing Advances in Wireless Communications (SPAWC),* 2011, pp. 381–385.

[7] Marzetta, Thomas L. "Noncooperative cellular wireless with unlimited numbers of base station antennas." *IEEE Transactions on Wireless Communications* 9.11 (2010): 3590-3600.

[8] Lee, Hyunjoong, Sangkyu Park, and Saewoong Bahk. "Enhancing Spectral Efficiency Using Aged CSI in Massive MIMO Systems." *Global Communications Conference (GLOBECOM)*, IEEE, 2016.

[9] Bai, Tianyang, and Robert W. Heath Jr. "Asymptotic coverage probability and rate in massive MIMO networks." *arXiv preprint arXiv*:1305.2233 (2013).

[10] Wu, D., and Negi, R., "Effective capacity: a wireless link model for support of quality of service", *IEEE Trans. Wirel. Commun.*,2, (4), pp. 630–643, 2003.

[11] J. Tang and X. Zhang, "Cross-layer-model based adaptive resource allocation for statistical QoS guarantees in mobile wireless networks," *IEEE Trans. Wireless Commun.*, vol. 7, no. 6, pp. 2318–2328, Jun. 2008.